Simplify your imaging workflows

Make research imaging workflows accessible, traceable, and secure with Athena Software for Core Imaging Facilities.

Thermo Scientific™ Athena Software is a premium imaging data management platform designed for core imaging facilities that support materials science research.

Athena Software ensures traceability of images, metadata, and experimental workflows through an intuitive and collaborative web interface.

Find out more at **thermofisher.com/athena**

ThermoFisher SCIENTIFIC

ADVANCED OPTICAL MATERIALS
www.advopticalmat.de

Synergistic Molecular Engineering of Hole-Injecting Conducting Polymers Overcomes Luminescence Quenching in Perovskite Light-Emitting Diodes

*Soyeong Ahn, Young-Hoon Kim, Sungjin Kim, Jinwoo Park, Nannan Li, Jung-Min Heo, Joo Sung Kim, Dong Jin Kim, Byung Hee Hong, Jin Yong Lee, and Tae-Woo Lee**

Electroluminescence efficiency and operating stability of solution-processed perovskite light-emitting diodes (PeLEDs) are limited by luminescence quenching induced by indium or tin released from indium tin oxide (ITO) electrode upon deposition of highly acidic conventional hole injection layer (HIL) (i.e., poly(3,4-ethylenedioxythiophene):poly(styrene sulfonate) (PEDOT:PSS)) and inefficient hole injection into perovskite emitting layer. Here, a synergistic molecular strategy to develop a neutralized gradient HIL, which possesses low acidity and high work function (*WF*) simultaneously, is proposed. First, it is shown that aniline with relatively low basicity and dipole moment efficiently neutralizes HIL while maintaining its original confirmation and high *WF*. Both acidity-neutralizing aniline and *WF*-modifying agent (perfluorinated ionomer) are incorporated into PEDOT:PSS to achieve high pH ≈ 6 and *WF* > 5.8 eV, which suppresses etching of underlying ITO and luminescence quenching while maintaining efficient hole injection into perovskite emitting layer. With this synergetic molecular engineering, high current efficiency = 52.55 cd A^{-1} with extended operating lifetime is achieved in PeLEDs that use colloidal formamidinium lead bromide nanoparticle films. This result provides a simple and efficient way to develop efficient and stable PeLEDs in industrial displays and solid-state lighting.

1. Introduction

Organic–inorganic hybrid perovskites have great promise as a light emitter in light-emitting diodes due to high color-purity, low material cost, and solution processability.[1–3] Perovskite light-emitting diodes (PeLEDs) with high electroluminescence (EL) efficiency have been achieved by fine stoichiometry control,[4] grain size control,[4] defect passivation,[5] and formation of quasi-2D (Ruddlesden–Popper phase) structures[6] or colloidal nanoparticles.[7] However, 3D perovskite polycrystalline films still have small exciton binding energy (e.g., ≈0.013 eV for methylammonium lead iodide, ≈0.04 eV for methylammonium lead bromide ($MAPbBr_3$)) which induces direct dissociation of electron–hole pairs into free charge carriers and severe luminescence quenching in the PeLEDs.[8,9] Therefore, preventing luminescence quenching in polycrystalline film based PeLEDs is of prime importance to increase their EL efficiency.

Dr. S. Ahn
Department of Materials Science and Engineering
Pohang University of Science and Technology (POSTECH)
77 Cheongam-Ro, Nam-Gu, Pohang
Gyeongbuk 790-784, Republic of Korea

Dr. S. Ahn, Dr. Y.-H. Kim, S. Kim, J. Park, J.-M. Heo, J. S. Kim, Prof. T.-W. Lee
Department of Materials Science and Engineering
Seoul National University
1 Gwanak-ro, Gwanak-gu, Seoul 08826, Republic of Korea
E-mail: twlees@snu.ac.kr

Dr. N. Li, Prof. J. Y. Lee
Department of Chemistry
Sungkyunkwan University
Suwon 16419, Republic of Korea

The ORCID identification number(s) for the author(s) of this article can be found under https://doi.org/10.1002/adom.202100646.

DOI: 10.1002/adom.202100646

Dr. D. J. Kim
Program in Nano Science and Technology
Graduate School of Convergence Science and Technology
Seoul National University
1 Gwanak-ro, Gwanak-gu, Seoul 08826, Republic of Korea

Dr. D. J. Kim, Prof. B. H. Hong
Graphene Research Center
Advanced Institute of Convergence Technology
Suwon 16229, Republic of Korea

Prof. B. H. Hong
Department of Chemistry
Seoul National University
1 Gwanak-ro, Gwanak-gu, Seoul 08826, Republic of Korea

Prof. T.-W. Lee
School of Chemical and Biological Engineering
Research Institute of Advanced Materials
Institute of Engineering Research
Nano Systems Institute (NSI)
Seoul National University
1 Gwanak-ro, Gwanak-gu, Seoul 08826, Republic of Korea

 © 2021 Wiley-VCH GmbH

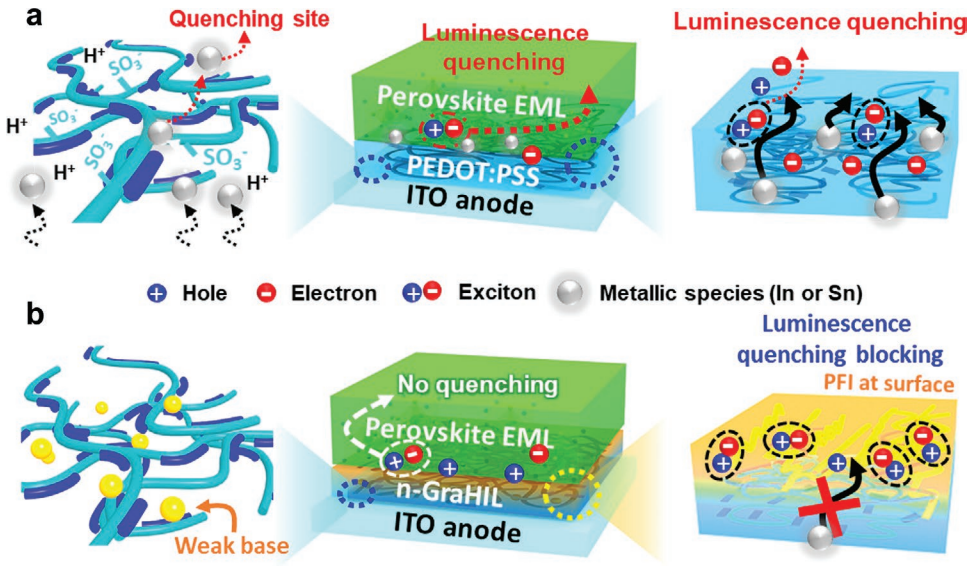

Figure 1. Schematic illustrations of a) luminescence quenching induced by metallic species diffused from ITO/PEDOT:PSS and b) suppressed metal diffusion and prevented luminescence quenching in ITO/n-GraHIL.

The luminescence quenching in polycrystal-PeLEDs mainly occurs at the interface between poly(3,4-ethylenedioxythiophene):poly(styrene sulfonate) (PEDOT:PSS) hole injection layer (HIL) and perovskite light-emitting layer.[3] Moreover, indium (In) and tin (Sn) species which are released from indium tin oxide (ITO) upon deposition of highly acidic PEDOT:PSS (pH = 1–2) migrate to the overlying perovskite emitting layer and further induce luminescence quenching (**Figure 1**a).[10] Moreover, a large energy-band offset between work function (*WF*) of PEDOT:PSS (4.8–5.2 eV) and valence band maximum (VBM) of perovskites (5.6–6.1 eV) induces inefficient injection and accumulation of holes at the PEDOT:PSS/perovskite interfaces.[11] These severe luminescence quenching and hole accumulation seriously limit the EL efficiency and operating stability of PeLEDs.

Suppression of hole accumulation at the PEDOT:PSS/perovskite interface have been tried by incorporating small additives (e.g., MoO_3-ammonia,[12] polar alcohol solvent,[13] dimethyl sulfoxide (DMSO), and Triton X-100[14]) into PEDOT:PSS. Moreover, luminescence quenching as well as hole accumulation were mitigated by adding nonconductive fluorosurfactant dopant in the PEDOT:PSS.[15] However, these strategies showed limited EL efficiency in PeLEDs (*CE* = 33.18 cd A^{-1}, external quantum efficiency (*EQE*) = 7.41%)[15] due to lack of comprehensive molecular engineering and fundamental analysis of additive effects on the interfaces. Moreover, these additives still cannot efficiently reduce the acidity of PEDOT:PSS and prevent the release of In and Sn from ITO, which still induces severe luminescence quenching in the PeLEDs. Therefore, solution-processed HIL which simultaneously facilitates hole injection into perovskite layer, has low acidity to prevent release of In and Sn from ITO and prevents luminescence quenching at the interface should be developed.

To prevent luminescence quenching and facilitate hole injection simultaneously, molecular approaches, which achieve low acidity and high *WF* in HIL, using at least two molecular additives are essential. Adding multiple molecular additives in conducting polymers often leads to change of polymer chain conformation and film morphology so that achieving both low acidity and high *WF* by two different molecular additives in PEDOT:PSS can be difficult without compromising the original film characteristics.

Here, we demonstrate highly efficient PeLEDs by synergistic molecular engineering of conducting polymer composition to develop neutralized gradient HIL (n-GraHIL)[16,17] which efficiently prevents the luminescence quenching in the PeLEDs (Figure 1b). First, we incorporate both *WF*-modifying agent (perfluorinated ionomer (PFI)) and acidity-neutralizing weak base additive (aniline) into the PEDOT:PSS. Incorporated co-additives efficiently neutralized the PEDOT:PSS (pH ≈ 6) while maintaining the high *WF* (>5.8 eV), which prevents luminescence quenching and facilitates charge injection at the HIL/perovskite interface simultaneously. By combining photophysical and chemical experiments with ab-initio molecular simulations, we studied how the basicity of the base additives affects the *WF* and acidity of the HILs and the luminescence quenching at the HIL/perovskite interface. Finally, we achieved *CE* = 17.16 cd A^{-1} in PeLEDs that use $MAPbBr_3$ polycrystalline bulk films and *CE* = 52.55 cd A^{-1} in PeLEDs that use colloidal formamidinium lead bromide ($FAPbBr_3$) nanoparticle films, both of which had extended operating lifetime.

2. Results and Discussion

First, we incorporate PFI into the PEDOT:PSS to facilitate hole injection into the perovskite emitting layer. PFI has lower surface energy (20 mN m^{-2}) than does PEDOT:PSS (38 mN m^{-2}). The low surface energy of PFI induces gradual increase of PFI concentration from the bottom surface to the top surface during the spincoating; this HIL composite film is called a GraHIL. The surface-enriched PFI induces a high *WF* ≈ 5.9 eV in

© 2021 Wiley-VCH GmbH

GraHIL.[16,17] Although GraHIL can prevent the luminescence-quenching at the PEDOT:PSS/perovskite emitting layer interface due to surface-enriched PFI,[3] GraHIL still has high acidity (pH ≈ 2.2) which induces etching of underlying ITO electrode and release of In and Sn species which act as luminescence quenching sites. Therefore, we added several different weak base additives to achieve a n-GraHIL. Additives usually disturb the self-organization of polymer blends due to molecular interactions,[18] so the PFI enrichment on the top surface of GraHIL can be severely affected by the additional additives. Therefore, in general, maintaining a high *WF* in GraHIL can be quite difficult once an additive has been incorporated.

Here, we evaluate three base additives which have different basicity but similar molecular structure to only consider the effects of basicity of additives by excluding other effects such as effects by molecular structure of additives: aniline (pK_a = 4.6), imidazole (pK_a = 7.0), and 2,3-dihydroxypyridine (DOH) (pK_a = 8.7) (**Figure 2**a). All n-GraHIL solutions with different base additives (aniline, imidazole, and DOH) showed pH that increases as a function of additive concentration and saturates (pH ≈ 6 for aniline, ≈7 for imidazole, and ≈10 for DOH) when the amount of additive is >1.5 mol% (Figure 2b). When imidazole and DOH are incorporated, the n-GraHIL showed seriously decreased *WF* ≈ 5.3 eV and ≈5.28 eV, respectively, compared to GraHIL (*WF* ≈ 5.8 eV) because basic additives disturb the self-organization of PFI on the surface of n-GraHIL, as expected.[18] However, when aniline is added, the n-GraHIL retains a surprisingly high *WF* > 5.8 eV.

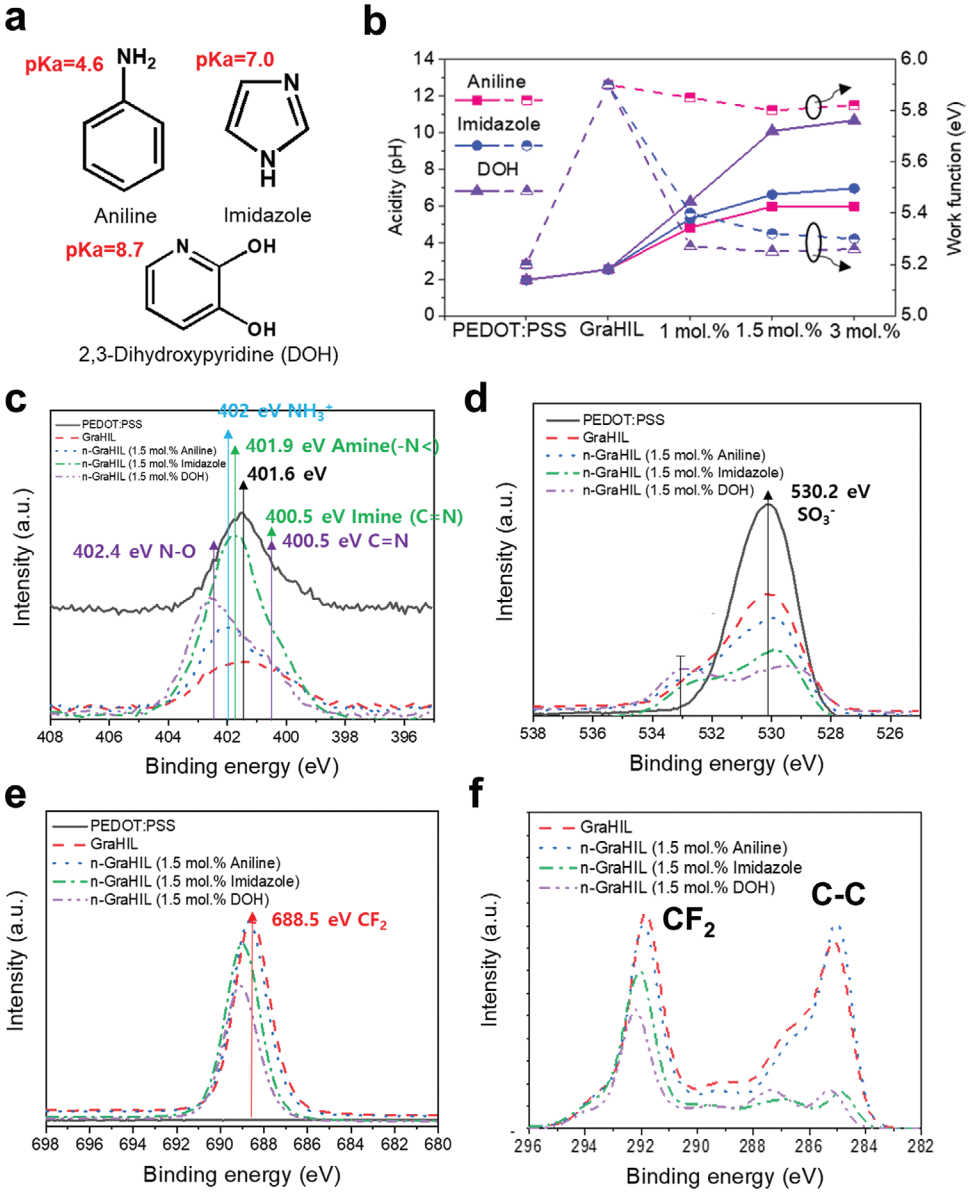

Figure 2. a) Molecular structure and basicity of aniline, imidazole, and 2,3-dihydroxypyridine (DOH). b) Acidity and *WF* of PEDOT:PSS, GraHIL, and n-GraHIL with various concentration of different base additives (aniline, imidazole, and DOH). XPS spectra of c) N 1s, d) O 1s, e) F 1s, and f) C 1s peak in PEDOT:PSS, GraHIL, and n-GraHIL with various base additives (aniline, imidazole, and DOH).

© 2021 Wiley-VCH GmbH

To investigate the effects of base additives on the *WF* and acidity of n-GraHIL, we conducted X-ray photoelectron spectroscopy (XPS) of PEDOT:PSS, GraHIL, and n-GraHIL with 1.5 mol% of aniline, imidazole, and DOH. n-GraHIL shows an intense N 1s peak that shifts to higher binding energy (402 eV for aniline, 401.9 eV for imidazole, and 402.4 eV for DOH) compared to the N 1s peak of PEDOT:PSS and GraHIL (401.6 eV), which represents the presence of basic additives on the top of n-GraHIL (Figure 2c). n-GraHIL with high basicity additives (pK_a = 7.0 for Imidazole, pK_a = 8.7 for DOH) showed higher calibrated N 1s peak intensity, in which measured N 1s peak was normalized by maximum C 1s peak intensity, than did aniline; this result indicates that additives with high basicity more largely are positioned on the top-surface of n-GraHIL by replacing PFI and PSS (Figure S1, Supporting Information). Furthermore, as the basicity of additive increases (from pK_a = 4.6 for aniline to pK_a = 8.7 for DOH), n-GraHIL shows decreasing peak intensities at ≈530.2 eV (O 1s peak representing SO_3^- (S—O) in PSS) (Figure 2d), at ≈688.5 eV (F 1s peak representing CF_2 in PFI) (Figure 2e), at ≈292 eV (C 1s peak representing CF_2 in PFI), and at ≈285 eV (C 1s peak representing aliphatic C—C in PSS chains) (Figure 2f). These indicate that basic additives with high basicity have high binding energy with PSS and PFI, more strongly interact with them, disturb self-organization of PSS and PFI to be located on the top-surface, and thus reduce their concentration on the top-surface, which result in low *WF* in n-GraHIL (Figure 2b).

To elucidate the interaction between basic additives and sulfonic acid groups in PSS and PFI, we calculated molecular dipole moment of additives and binding energies (ΔE) between each basic additive and PSS or PFI, by performing density functional theory (DFT) calculations as implanted in the Gaussian 16 package. As the basicity of additive increases, their dipole moment increases (1.66 D for aniline, 3.89 D for imidazole, and 5.13 D for DOH) (**Figure 3**a). The binding energy (eV) is calculated as

$$\Delta E = E_{total} - E_{cation} - E_{anion} \quad \text{or} \quad \Delta E = E_{total} - E_{molecule} - E_{anion} \tag{1}$$

where E_{total} is the total energy of the molecular combination, E_{cation} is the energy of the cation, E_{anion} is the energy of the anion, and $E_{molecule}$ is the energy of the molecule of each combination. Here, a negative value for binding energy represents strong binding between the fragments. For the binding energy calculation of $PEDOT^+$:PSS^-, three units of PEDOT with one unit of PSS were considered. For simplicity, the smallest PFI molecule was used. As the basicity and dipole moment of additive increased, the magnitude of the difference between the binding energies of basic additives and PSS or PFI gradually increased (–65 kJ mol^{-1} for aniline-PSS, –93 kJ mol^{-1} for imidazole-PSS, and –101 kJ mol^{-1} for DOH-PSS; –53 kJ mol^{-1} for aniline-PFI, –77 kJ mol^{-1} for imidazole-PFI, and –83 kJ mol^{-1} for DOH-PFI) (Figure 3b); this tendency corroborates the results of low *WF* and decreased XPS peak intensities of PSS and PFI signals in the n-GraHIL with imidazole and DOH (Figure 2). This strong interaction between high-basicity additives (imidazole and DOH) and PSS induces severe phase separation between PEDOT and PSS, and increases the propensity for aggregation of the film morphology (Figures S2,S3, Supporting Information).[19] The combination of *WF* change, XPS spectroscopy, and DFT simulation indicates that aniline has weak interaction with PFI and PSS and thus can maintain original conformation and organization of GraHIL, which result in high *WF* ≈ 5.8 eV while effectively neutralizing the acidity (pH ≈ 6) and preventing the luminescence quenching. Therefore, we now investigate the effects of aniline in n-GraHIL on the 1) suppressed etching of underlying electrodes, 2) prevented luminescence quenching at the interface, and 3) increased EL efficiency and operating stability in PeLEDs.

To visualize the effect of aniline on the corrosion of the underlying layer that n-GraHIL contacts, we placed droplets of HIL solutions (PEDOT:PSS, GraHIL, and n-GraHIL with 1.0,

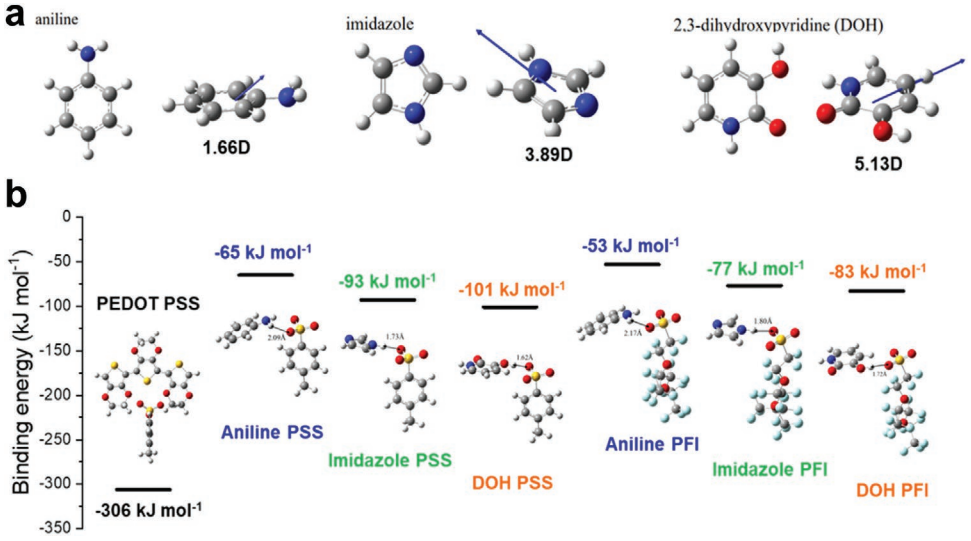

Figure 3. a) Simulated molecular structures and dipole moments of each base additives (aniline, imidazole, and DOH). The direction of their dipole moment is also shown as blue arrow. b) Calculated binding energies between various base additives (aniline, imidazole, and DOH) and PSS or PFI. The distance between the two fragments is also shown.

© 2021 Wiley-VCH GmbH

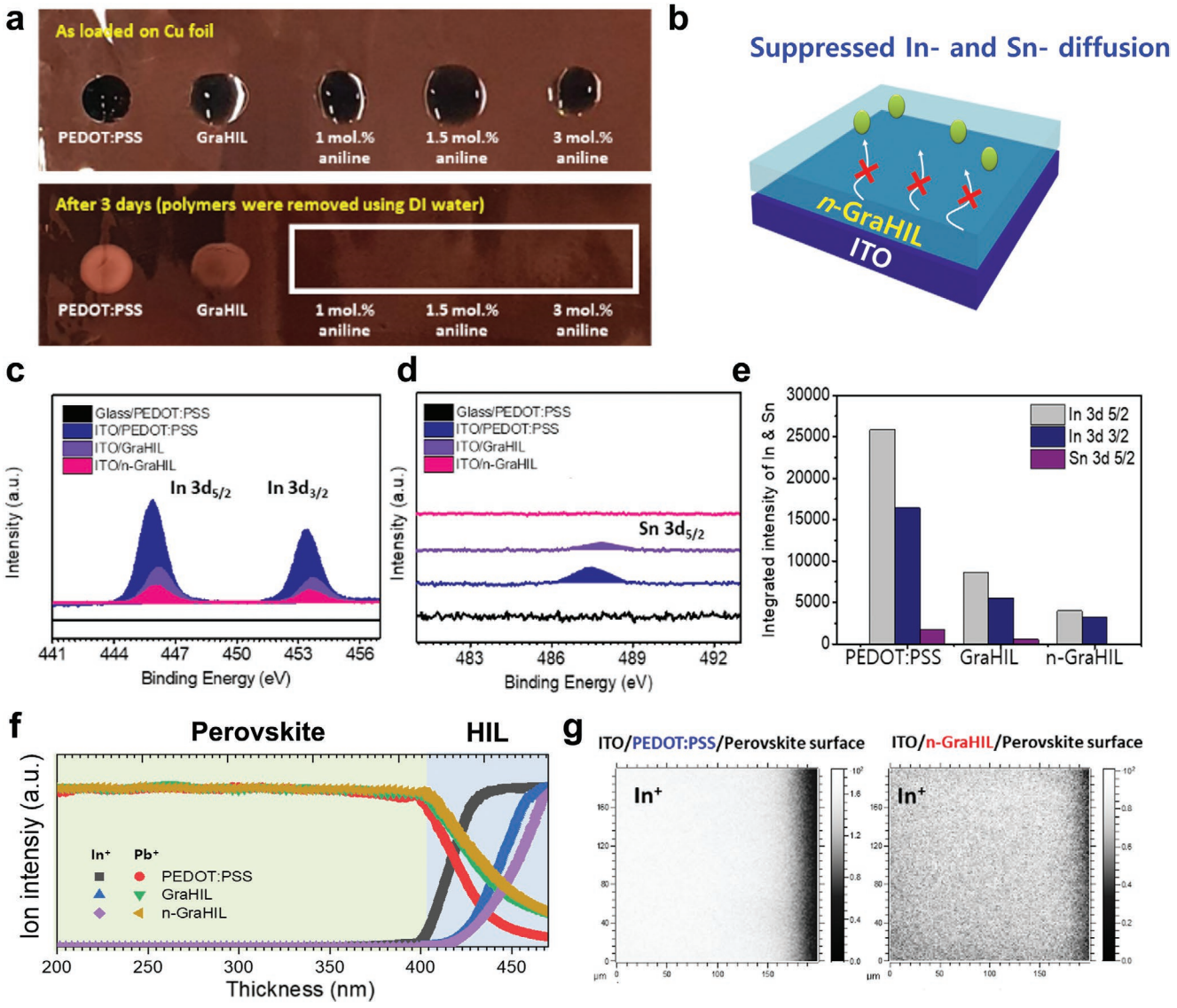

Figure 4. a) Photographs of HIL droplets (PEDOT:PSS, GraHIL, and n-GraHIL with 1.0, 1.5, and 3.0 mol% of aniline) on a Cu foil. b) Schematic illustrations of suppressed diffusion of metallic species (In, Sn) in ITO/n-GraHIL. XPS spectra of c) In 3d and d) Sn 3d peaks and e) integrated intensity measured on glass/PEDOT:PSS, ITO/PEDOT:PSS, ITO/GraHIL, and ITO/n-GraHIL. f) Depth-profiling TOF-SIMS spectra and g) In^+ images of ITO/PEDOT:PSS or GraHIL or n-GraHIL/$MAPbBr_3$ bulk films.

1.5, or 3.0 mol% aniline) on a copper foil and left them for 3 days (**Figure 4a**). PEDOT:PSS and GraHIL droplets chemically etched the copper foil, whereas n-GraHIL did not due to its neutralized acidity (pH ≈ 6) (Figure 4b).

To investigate the suppressed chemical etching of underlying layer by n-GraHIL, we first conducted XPS on the surface of various samples (glass/PEDOT:PSS for control experiment, ITO/PEDOT:PSS or GraHIL or n-GraHIL with 1.5 mol% aniline). The ITO/PEDOT:PSS sample (pH ≈ 1.8) showed strong In $3d_{5/2}$ peak at ≈ 445.5 eV, In $3d_{3/2}$ peak at ≈453.3 eV, and Sn $3d_{3/2}$ peak at ≈487.5 eV due to the etching of underlying ITO and concomitant release of In ions and Sn ions (Figure 4c–e). The ITO/GraHIL sample (pH ≈ 2.2) still showed In $3d_{3/2}$ and Sn $3d_{3/2}$ peaks which are smaller than those in the ITO/PEDOT:PSS sample. However, n-GraHIL showed significantly reduced In $3d_{5/2}$ and In $3d_{3/2}$ peaks and no Sn peak due to lower acidity (pH ≈ 6) than PEDOT:PSS (pH ≈ 1.8) and GraHIL (pH ≈ 2.2).

To quantify the diffusion of In and Sn toward the overlying perovskite layer through various HILs, we performed time-of-flight secondary ion mass spectrometry (TOF-SIMS) depth-profiling on various samples (ITO/PEDOT:PSS or GraHIL or n-GraHIL/$MAPbBr_3$ polycrystalline bulk films). All three samples showed Pb signals in the HILs possibly due to the partial intermixing between perovskite layers and HILs (Figure 4f). ITO/PEDOT:PSS/$MAPbBr_3$ showed an intense In signal at the HIL/$MAPbBr_3$ interface and even on the top surface of the $MAPbBr_3$ layer (Figure 4f,g). On the contrary, ITO/GraHIL or n-GraHIL/$MAPbBr_3$ showed significantly reduced density of In signal both at the HIL/$MAPbBr_3$ interface and on the top of the $MAPbBr_3$ layer.

© 2021 Wiley-VCH GmbH

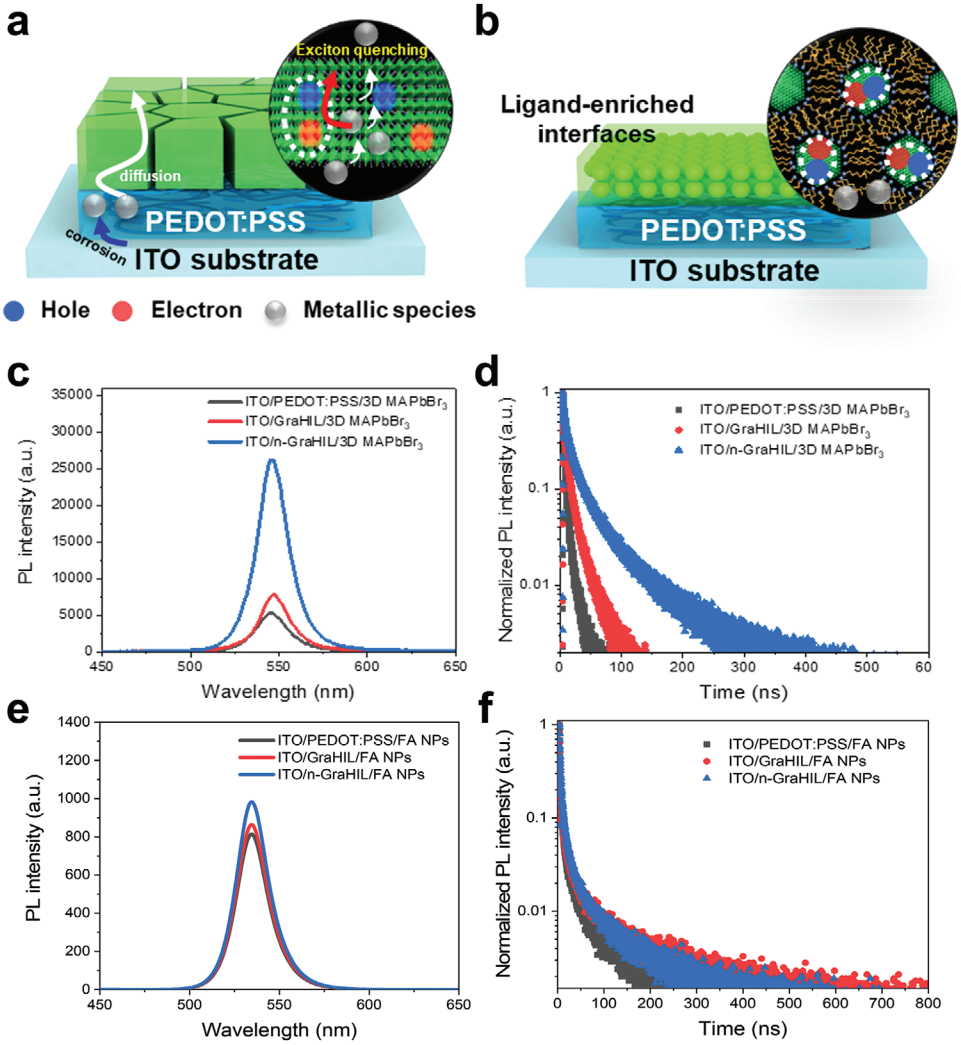

Figure 5. Schematic illustrations of luminescence quenching in a) ITO/PEDOT:PSS/$MAPbBr_3$ polycrystalline bulk film and b) ITO/PEDOT:PSS/$FAPbBr_3$ nanoparticle film. Here, $FAPbBr_3$ nanoparticle films have less luminescence quenching than do $MAPbBr_3$ polycrystalline bulk films due to higher exciton binding energy. PL intensity and lifetime of c,d) $MAPbBr_3$ polycrystalline bulk films and e,f) $FAPbBr_3$ nanoparticle films on various under layers (ITO/PEDOT:PSS or GraHIL or n-GraHIL).

To study the effects of co-additives (PFI, aniline) on the luminescence quenching in the perovskite emitting layers, we measured steady-state photoluminescence (PL) and PL lifetime of perovskite films on top of various HILs (ITO/PEDOT:PSS or GraHIL or n-GraHIL/$MAPbBr_3$ polycrystalline bulk films or colloidal $FAPbBr_3$ nanoparticle films) (**Figure 5**a,b). Here, considering the two research subfields (i.e., polycrystalline films, colloidal nanoparticles) that apply to PeLEDs, we tested two different perovskite films ($MAPbBr_3$ polycrystalline films and colloidal $FAPbBr_3$ nanoparticle films). In both polycrystalline films and nanoparticle films, the PL intensity and the PL lifetime increased as the acidity of the HIL film decreased (pH of the HIL increases from ≈1.8 for PEDOT:PSS, to ≈2.2 for GraHIL, to ≈6 for n-GraHIL) (Figure 5c–f). The HILs did not affect the morphology or crystal structure of $MAPbBr_3$ polycrystalline films (Figure S4, Supporting Information), so we attribute the increased PL intensity and PL lifetime to the suppressed release of metallic species from the ITO and concomitant reduced luminescence quenching. We mention that aniline in the n-GraHIL can diffuse into the perovskite layers upon the loading and spincoating of perovskite solutions and contribute to the increases of steady-state PL intensity and PL lifetime, as other underlying interlayer did on perovskite films.[20,21] Here, larger increases of PL intensity and lifetime in polycrystalline films than in nanoparticle films can be attributed to the smaller exciton binding energy and thus much easier luminescence quenching in polycrystalline films than in nanoparticle films (magnified illustrations in Figure 5a,b).

Aniline can also affect the electrical conductivity of PEDOT:PSS and GraHIL. Here, we used Clevios PH500 as a PEDOT:PSS because it has high conductivity (1.69 S cm^{-1}) which is easy for characterization. Incorporating 1.5 mol% aniline into the PH500 or GraHIL (here, PH500:PFI) increased the conductivity from 1.69 to 25.1 S cm^{-1} in the PH500, and from 1.81 to 32.2 S cm^{-1} in the GraHIL (Figure S5, Supporting Information).

© 2021 Wiley-VCH GmbH

To investigate the reason for the increase in conductivity by the aniline additive, we conducted Raman spectroscopy measurements on PEDOT:PSS and GraHIL with 0, 1.0, 1.5, or 3.0 mol% aniline (Figure S6, Supporting Information). Both PEDOT:PSS and GraHIL showed Raman peaks at 1438 cm^{-1}, which is attributed to C_α–C_β symmetric stretching. As the concentration of added aniline increased, Raman spectra in both n-PEDOT:PSS and n-GraHIL gradually shifted toward lower wavenumber. These shifts indicate a structural change from benzoid to quinoid of thiophene ring in the PEDOT chains.[22,23] The structural change of thiophene ring induces a conformational change of conjugated chains from coiled to linear, which is confirmed by elongated PEDOT domains when 1.5 mol% of aniline is incorporated (Figure S7a–c,e–g, Supporting Information). These linearly-conjugated chains (elongated PEDOT domains) permit an increase in the number of electron that can be delocalized through the neighboring thiophene rings, and can favor the conduction of charge carriers; these changes increase the electrical conductivity. However, when excessive aniline is incorporated (3 mol%), the PEDOT domains agglomerate and the conductivity of the HIL suddenly decreases (Figures S5,S7d,h, Supporting Information). These findings suggest that addition of aniline not only reduces the acidity of HILs and luminescence quenching but also increases its electrical conductivity by inducing elongated PEDOT domains and consequently delocalizing electrons on the PEDOT chains. The fact that addition of aniline suppresses the luminescence quenching despite increased electrical conductivity in n-GraHIL indicates that metallic species (In, Sn) released from ITO are the main reason of luminescence quenching over conductivity of HILs.

To study the effects of PFI and aniline additives on the luminous characteristics of PeLEDs, we fabricated PeLEDs that used $MAPbBr_3$ polycrystalline bulk films and $FAPbBr_3$ nanoparticle films, both are combined with PEDOT:PSS, GraHIL, or n-GraHIL with 1.5 mol% aniline (**Figure 6**a,b). Device efficiency and operating stability are summarized in Tables S1,S2, Supporting Information. PeLEDs with GraHIL showed increased device efficiencies and maximum luminance L_{max} ($CE \approx 12$ cd A^{-1}, $EQE \approx 2.42\%$, and $L_{max} \approx 20\,010$ cd m^{-2} for PeLEDs that use $MAPbBr_3$ polycrystalline bulk films; $CE \approx 52.3$ cd A^{-1}, $EQE \approx 11.4\%$, and $L_{max} \approx 11\,679$ cd m^{-2} for PeLEDs that use $FAPbBr_3$ nanoparticle films) than those with conventional PEDOT:PSS ($CE \approx 7.02$ cd A^{-1}, $EQE \approx 1.52\%$, and $L_{max} \approx 2358$ cd m^{-2} for PeLEDs that use $MAPbBr_3$ polycrystalline bulk films; $CE \approx 28$ cd A^{-1}, $EQE \approx 6.04\%$, and $L_{max} \approx 1052$ cd m^{-2} for PeLEDs that use $FAPbBr_3$ nanoparticle films) (Figure 6c–f). PeLEDs that had the n-GraHIL showed further increased device performances (CE ≈ 17.16 cd A^{-1}, $EQE \approx 3.7\%$, and $L_{max} \approx 44\,858$ cd m^{-2} for PeLEDs that use $MAPbBr_3$ polycrystalline bulk films; CE ≈ 52.55 cd A^{-1}, $EQE \approx 11.5\%$, and $L_{max} \approx 15010$ cd m^{-2} for PeLEDs that use $FAPbBr_3$ nanoparticle films). These efficiency tendencies of PeLEDs that use $MAPbBr_3$ polycrystalline bulk films and $FAPbBr_3$ nanoparticle films are reproducible (Figure S8, Supporting Information). Furthermore, PeLEDs that use $MAPbBr_3$ polycrystalline films with n-GraHIL showed turn-on voltage of ≈3 V at 10 cd m^{-2} which is lower than those with GraHIL (≈3.5 V) and PEDOT:PSS (≈4.5 V).

PeLEDs with n-GraHIL showed operating stability (half lifetime in which initial luminance (100 cd m^{-2}) decreases to 50%, $L_{50} \approx 2.2$ h for PeLEDs that use $MAPbBr_3$ polycrystalline bulk films and $L_{50} \approx 27$ min for PeLEDs that use $FAPbBr_3$ nanoparticle films) which are longer than did those with GraHIL ($L_{50} \approx 1.2$ h for PeLEDs that use $MAPbBr_3$ polycrystalline bulk films; $L_{50} \approx 11.2$ min for PeLEDs that use $FAPbBr_3$ nanoparticle films) and those with PEDOT:PSS ($L_{50} \approx 0.65$ h for PeLEDs that use $MAPbBr_3$ polycrystalline bulk films; $L_{50} \approx 9$ min for PeLEDs that use $FAPbBr_3$ nanoparticle films). Here, we attribute the severe luminance overshoot in PeLEDs based on $MAPbBr_3$ polycrystalline bulk films to the ion-migration in the polycrystalline films. These results indicate that synergetic additive incorporation of PFI and aniline into PEDOT:PSS HIL suppresses migration of In and Sn species from ITO electrode and thus increases both device efficiency and operating stability in PeLEDs.

3. Conclusion

We obtained a neutralized (pH ≈ 6) gradient polymer HIL (n-GraHIL) that has high *WF* (>5.8 eV) and suppresses the luminescence quenching in PeLEDs. The n-GraHIL was obtained by synergistic molecular engineering to incorporate both acidity-neutralizing weak base additive (aniline) and *WF*-modifying agent (PFI) into PEDOT:PSS. The high dipole moment of basic additives changes the conformation of polymer blends: if the basic additive has excessively strong dipole moment, it induces severe lateral phase separation and interfere vertical segregation of PFI, which decrease the *WF* of the HIL. Therefore, we chose aniline as a weak base additive to reduce acidity while keeping an original conformation and high *WF* in n-GraHIL. As a result, the amounts of metallic species (i.e., In, Sn) released from the ITO anode and luminescence quenching in the devices were significantly reduced and n-GraHIL maintained high $WF \approx 5.8$ eV. Inclusion of aniline in the HIL also increased the electrical conductivity by elongating the PEDOT:PSS domains in the PEDOT:PSS. Ultimately, we achieved high $CE \approx 52.55$ cd A^{-1} and extended device lifetime ($L_{50} \approx 27$ min) in colloidal $FAPbBr_3$ nanoparticle based PeLEDs with n-GraHIL, which are much higher than those obtained using conventional PEDOT:PSS ($CE \approx 28$ cd A^{-1}, $L_{50} \approx 9$ min). This work highlights the importance of controlling the acidity and *WF* of HILs in PeLEDs and suggests a simple way to reduce luminescence quenching and increase hole injection in PeLEDs.

4. Experimental Section

Materials: PEDOT:PSS (Clevios PH500) was purchased from Heraeus, PSS was purchased from Heraeus, and PFI was purchased from Sigma Aldrich. Aniline > 99.5%, imidazole > 99%, and 2,3-dihydroxypyridine > 95% were purchased from Sigma Aldrich. Methylammonium bromide (MABr) and formamidinium bromide (FABr) were purchased from Dyesol. Lead bromide ($PbBr_2$) and DMSO were purchased from Sigma Aldrich. All were used without further purification.

Measurements: pH of conducting polymer solutions were measured using a bench-top pH meter (Thermo Scientific Orion Star A215 pH/conductivity meter). *WF*s of the polymer films were evaluated using a Kelvin probe system (KP technologies Ltd.). Atomic force microscope

© 2021 Wiley-VCH GmbH

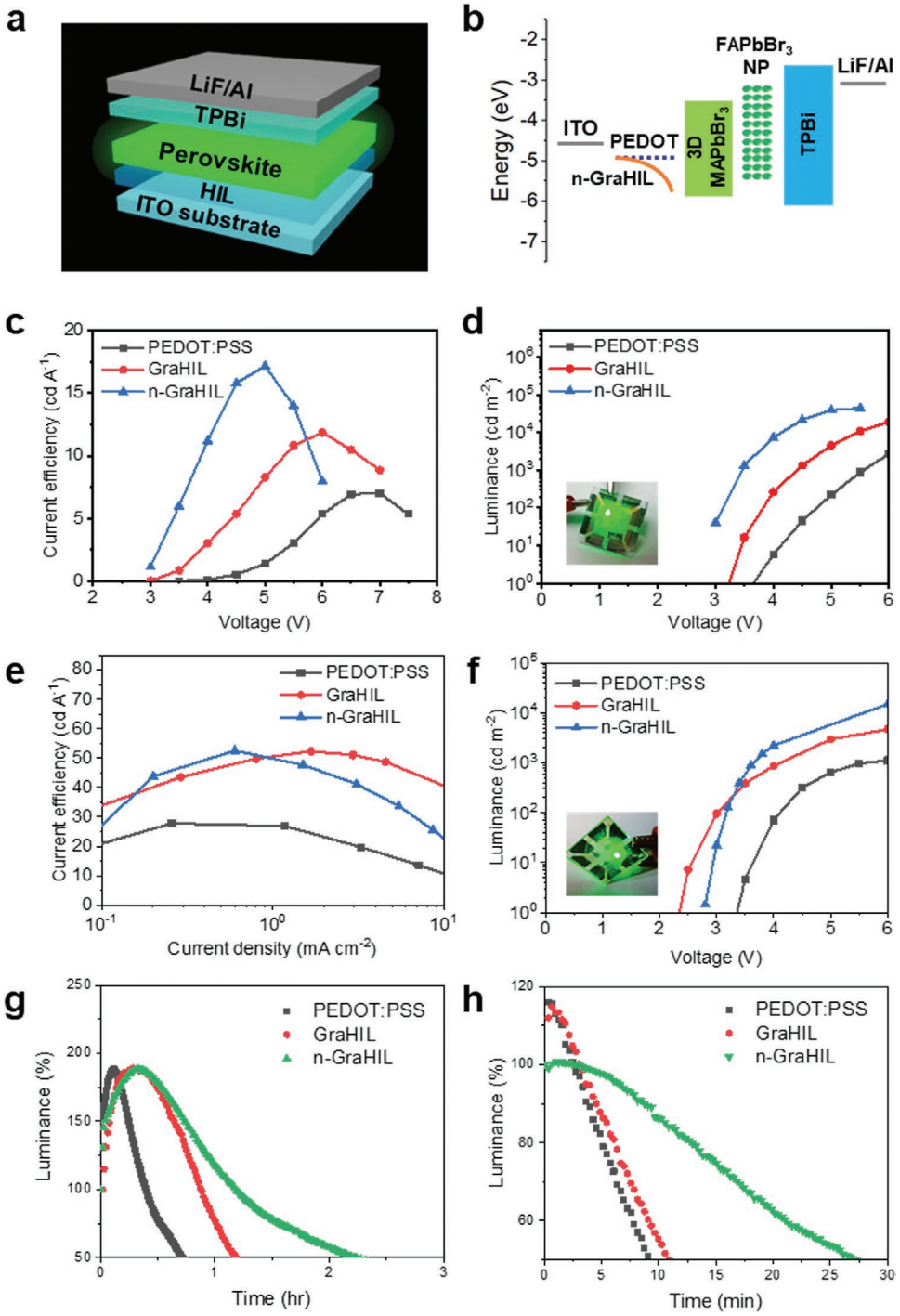

Figure 6. a) Device structure and b) energy band diagram of PeLEDs using different HILs (PEDOT:PSS, GraHIL, and n-GraHIL) and two different perovskite emitting layers ($MAPbBr_3$ polycrystalline bulk film, $FAPbBr_3$ nanoparticle film). c) Current efficiency and d) luminance characteristics of PeLEDs based on $MAPbBr_3$ polycrystalline bulk films with different HILs (PEDOT:PSS, GraHIL, and n-GraHIL). e) Current efficiency and f) luminance characteristics of PeLEDs based on $FAPbBr_3$ nanoparticle films with different HILs (PEDOT:PSS, GraHIL, and n-GraHIL). Device lifetime, which was measured at initial luminance of 100 cd m^{-2}, of g) PeLEDs based on $MAPbBr_3$ polycrystalline bulk films and h) PeLEDs based on $FAPbBr_3$ nanoparticle films with different HILs (PEDOT:PSS, GraHIL, and n-GraHIL).

(AFM) images were obtained using an AFM NX-10 (Park Systems). Scanning electron microscope (SEM) images were captured using a field-emission SEM (SUPRA 55VP, Carl Zeiss). Raman spectra were collected using a micro-Raman spectrometer (Renishaw) with a 514-nm Ar laser. TOF-SIMS measurements were obtained using a TOF-SIMS 5 (ION-TOF GmbH, Münster, Germany) at the Korea Basic Science Institute Busan Center by using a pulsed 30-keV Bi^{3+} primary beam with a current of 0.29 A. The area used for analysis was a square of 200 μm × 200 μm. Positive-ion spectra were internally calibrated using H^+, CH_3^+, $C_2H_5^+$, $C_3H_7^+$, and $C_4H_9^+$ normalized to the respective secondary total ion

© 2021 Wiley-VCH GmbH

yields. The depth profile was a square of 500 μm × 500 μm using Ar-cluster 5 keV. Steady-state PL of OHP films was measured using a spectrofluorometer (JASCO FP8500, Jasco International Co., Ltd., Japan) and the PL lifetimes were collected using a fluorescence spectrometer (FluoTime 300). A picosecond-pulse laser head (LDH-P-C-405B, PicoQuant) was used as an excitation source (wavelength: 405 nm), and photon-counting detector (PMA Hybrid 07) and a time-correlated single-photon counting module (PicoHarp, PicoQuant) were used to detect the PL lifetimes of OHP samples.

Density Functional Theory Calculation: All DFT calculations in this study were performed using the Gaussian 16 package. The PBE0 exchange correlation functional and 6-31++G(d,p) basis sets were used for the molecular structure optimization.

Preparation of Perovskite Precursor and Nanoparticle Solution: To prepare polycrystalline $MAPbBr_3$ precursor solution (40 wt%), MABr and $PbBr_2$ were dissolved in DMSO in a molar ratio of MABr:$PbBr_2$ = 1.06:1 at room temperature, then the solution was stirred for ≥3 h. $FAPbBr_3$ nanoparticles were synthesized using ligand-assisted reprecipitation following previous literature[24] with the modification.

PeLED Fabrication: ITO-patterned glass substrates were cleaned by sequential ultrasonication in acetone for 15 min and isopropyl alcohol in 15 min, then exposed to UV-ozone for 20 min. Then the HILs were formed by spin-coating at 4500 rpm for 90 s and baking at 150 °C for 30 min on a hotplate. The ITO/HIL samples were transferred to a N_2-filled glove box to form OHP films. The 3D $MAPbBr_3$ polycrystalline bulk films were formed using additive-assisted nanocrystal pinning[4] and $FAPbBr_3$ nanoparticle films were fabricated by spincoating at 1000 rpm for 60 s. Then 2,2′,2″-(1,3,5-benzinetriyl)-tris(1-phenyl-1-H-benzimidazole) (50 nm), lithium fluoride (1 nm) and aluminum (100 nm) were sequentially deposited using a thermal evaporator in a high vacuum ($<10^{-7}$ Torr). The fabricated PeLEDs were encapsulated by a glass lid under dry N_2 atmosphere.

Supporting Information

Supporting Information is available from the Wiley Online Library or from the author.

Acknowledgements

S.A., Y.-H.K., and S.K. contributed equally to this work. This work was supported by the National Research Foundation of Korea (NRF) grant funded by the Korea government (MSIT) (NRF-2016R1A3B1908431).

Conflict of Interest

The authors declare no conflict of interest.

Data Availability Statement

Research data are not shared.

Keywords

acidity control, efficient hole injection, luminescence quenching, neutralization, organic–inorganic hybrid perovskites

Received: March 31, 2021
Revised: April 27, 2021
Published online:

[1] Y.-H. Kim, H. Cho, T.-W. Lee, *Proc. Natl. Acad. Sci. USA* **2016**, *113*, 11694.
[2] Z.-K. Tan, R. S. Moghaddam, M. L. Lai, P. Docampo, R. Higler, F. Deschler, M. Price, A. Sadhanala, L. M. Pazos, D. Credgington, F. Hanusch, T. Bein, H. J. Snaith, R. H. Friend, *Nat. Nanotechnol.* **2014**, *9*, 687.
[3] Y.-H. Kim, H. Cho, J. H. Heo, T.-S. Kim, N. Myoung, C.-L. Lee, S. H. Im, T.-W. Lee, *Adv. Mater.* **2015**, *27*, 1248.
[4] H. Cho, S.-H. Jeong, M.-H. Park, Y.-H. Kim, C. Wolf, C.-L. Lee, J. H. Heo, A. Sadhanala, N. Myoung, S. Yoo, S. H. Im, R. H. Friend, T.-W. Lee, *Science* **2015**, *350*, 1222.
[5] B. Zhao, S. Bai, V. Kim, R. Lamboll, R. Shivanna, F. Auras, J. M. Richter, L. Yang, L. Dai, M. Alsari, X.-J. She, L. Liang, J. Zhang, S. Lilliu, P. Gao, H. J. Snaith, J. Wang, N. C. Greenham, R. H. Friend, D. Di, *Nat. Photon.* **2018**, *12*, 783.
[6] M. Yuan, L. N. Quan, R. Comin, G. Walters, R. Sabatini, O. Voznyy, S. Hoogland, Y. Zhao, E. M. Beauregard, P. Kanjanaboos, Z. Lu, D. H. Kim, E. H. Sargent, *Nat. Nanotechnol.* **2016**, *11*, 872.
[7] Y.-H. Kim, S. Kim, A. Kakekhani, J. Park, J. Park, Y.-H. Lee, H. Xu, S. Nagane, R. B. Wexler, D.-H. Kim, S. H. Jo, L. Martínez-Sarti, P. Tan, A. Sadhanala, G.-S. Park, Y.-W. Kim, B. Hu, H. J. Bolink, S. Yoo, R. H. Friend, A. M. Rappe, T.-W. Lee, *Nat. Photon.* **2021**, *15*, 148.
[8] Y. Yang, M. Yang, Z. Li, R. Crisp, K. Zhu, M. C. Beard, *J. Phys. Chem. Lett.* **2015**, *6*, 4688.
[9] K. Tanaka, T. Takahashi, T. Ban, T. Kondo, K. Uchida, N. Miura, *Solid State Commun.* **2003**, *127*, 619.
[10] H.-K. Seo, H. Kim, J. Lee, M.-H. Park, S.-H. Jeong, Y.-H. Kim, S.-J. Kwon, T.-H. Han, S. Yoo, T.-W. Lee, *Adv. Mater.* **2017**, *29*, 1605587.
[11] Y.-H. Kim, C. Wolf, H. Cho, S.-H. Jeong, T.-W. Lee, *Adv. Mater.* **2016**, *28*, 734.
[12] Y. Meng, M. Ahmadi, X. Wu, T. Xu, L. Xu, Z. Xiong, P. Chen, *Org. Electron.* **2019**, *64*, 47.
[13] M. Wu, D. Zhao, Z. Wang, J. Yu, *Nanoscale Res. Lett.* **2018**, *13*, 128.
[14] Q. Zhang, Y. Lu, Z. Liu, H. Yu, Y. Duan, L. Liu, S. Chen, W. Huang, *Org. Electron.* **2019**, *72*, 30.
[15] S. Y. Lee, Y. S. Nam, J. C. Yu, S. Lee, E. D. Jung, S.-H. Kim, S. Lee, J.-Y. Kim, M. H. Song, *ACS Appl. Mater. Interfaces* **2019**, *11*, 39274.
[16] T.-W. Lee, Y. Chung, O. Kwon, J.-J. Park, *Adv. Funct. Mater.* **2007**, *17*, 390.
[17] T.-H. Han, Y. Lee, M.-R. Choi, S.-H. Woo, S.-H. Bae, B. H. Hong, J.-H. Ahn, T.-W. Lee, *Nat. Photon.* **2012**, *6*, 105.
[18] Y. J. Kim, S. Ahn, D. H. Wang, C. E. Park, *Sci. Rep.* **2015**, *5*, 18024.
[19] H. J. Oh, J. G. Jang, J.-G. Kim, J.-I. Hong, J. Kim, J. Kwak, S. H. Kim, S. Shin, *Sci. Rep.* **2017**, *7*, 13287.
[20] H. Wang, X. Gong, D. Zhao, Y.-B. Zhao, S. Wang, J. Zhang, L. Kong, B. Wei, R. Quintero-Bermudez, O. Voznyy, Y. Shang, Z. Ning, Y. Yan, E. H. Sargent, X. Yang, *Joule* **2020**, *4*, 1977.
[21] L. Xu, J. Li, B. Cai, J. Song, F. Zhang, T. Fang, H. Zeng, *Nat. Commun.* **2020**, *11*, 3902.
[22] S.-H. Jeong, H. Kim, M.-H. Park, Y. Lee, N. Li, H.-K. Seo, T.-H. Han, S. Ahn, J.-M. Heo, K. S. Kim, T.-W. Lee, *Nano Energy* **2019**, *60*, 324.
[23] T.-H. Han, W. Song, T.-W. Lee, *ACS Appl. Mater. Interfaces* **2015**, *7*, 3117.
[24] X. Y. Chin, A. Perumal, A. Bruno, N. Yantara, S. A. Veldhuis, L. Martínez-Sarti, B. Chandran, V. Chirvony, A. S.-Z. Lo, J. So, C. Soci, M. Grätzel, H. J. Bolink, N. Mathews, S. G. Mhaisalkar, *Energy Environ. Sci.* **2018**, *11*, 1770.

© 2021 Wiley-VCH GmbH